PERGAMON

International Journal of Heat and Mass Transfer 42 (1999) 3495–3507

International Journal of HEAT and MASS TRANSFER

Numerical simulation of vortex shedding past a circular cylinder under the influence of buoyancy

B.S. Varaprasad Patnaik[a, 1], P.A. Aswatha Narayana[a,*], K.N. Seetharamu[b]

[a]*Department of Applied Mechanics, IIT, Madras 600 036, India*
[b]*Department of Mechanical Engineering, IIT, Madras 600 036, India*

Received 15 November 1997; accepted 24 November 1998

Abstract

Flow past an isolated circular cylinder is numerically simulated, under the influence of aiding and opposing buoyancy. A modified velocity correction procedure is incorporated. Galerkin weighted residual formulation is employed for spatial discretization along with a second-order Runge–Kutta (R–K) time integration scheme. The influence of buoyancy on the Nusselt number, wake structures, temporal lift and drag forces have been studied. At low Reynolds numbers (for, e.g., $Re = 20$–40), buoyancy opposing the flow could trigger vortex shedding. The degeneration of the Kàrmàn vortex street into twin vortices is numerically simulated for a heated cylinder. The two zones of vortex shedding and twin vortices are demarcated.

1. Introduction

When flow takes place past a bluff body, the phenomenon of vortex shedding results over a wide range of Reynolds numbers. Flow past a circular cylinder is a very well investigated bench mark problem, and a vast amount of literature exists [1]. Vortex shedding becomes all the more complicated, when the buoyant forces are imparted over the viscous phenomenon. In measuring low fluid velocities, buoyancy effects on warm sensors become increasingly more important. In constant temperature anemometers, the sensor wire or film is maintained at a certain temperature above the fluid stream, whose velocity is to be measured. A knowledge of the heat transfer coefficients are certainly invaluable to designers in the development of instruments using wires such as thermo-elements and hot wire anemometers [2]. Further, this classical and practically interesting phenomenon has its implications in other application areas, such as heat exchanger tubes, nuclear reactor fuel rods, chimney stacks, cooling towers, offshore structures, etc., as the circular cylinder is a basic configuration. A number of engineering design parameters connected with fluid flow, heat transfer and vibration become important in these studies. Apart from the engineering relevance, a study of these mechanisms associated with the laminar flow past cylinders, forms the first step towards understanding the vastly more complicated phenomenon of turbulence [3].

Sharma and Sukhatme [4] have investigated the influence of free and forced convection heat transfer past a heated tube. Oösthuizen and Madan [5] have studied the influence of mixed convection over a Reynolds number range of 100–300. However, their interest was on the average heat transfer, but not on the detailed

* Corresponding author. Tel.: +91 44 235 1365; fax: +91 44 235 0509.

E-mail address: paa_iitm@hotmail.com (P.A. Aswatha Narayana)

[1] Present address: Department of Mechanical Engineering, UBC, Vancover, Canada V6T 1Z4.

0017-9310/99/$ - see front matter
PII: S0017-9310(98)00373-1

behavior of the near wake vortices. Joshi and Sukhatme [6] have employed a coordinate perturbation method to transform the governing set of partial differential equations into an ordinary form, and then solved it by a numerical scheme. The boundary layer flow assumption made in the numerical investigations, of Joshi and Sukhatme [6], Sparrow and Lee [7] and Merkin [8] has limited their prediction of the local Nusselt number distribution only upto the point of separation. Jain and Lohar [9] have pointed out an increase in vortex shedding frequency with an increase in cylinder temperature. For a heated cylinder, Noto and Matsumoto [10] have investigated the degeneration of the Kàrmàn vortex street. Chang and Sa [11] have reported a detailed study on the vortex mechanisms in the near wake of a heated/cooled circular cylinder by a finite difference scheme. They have employed a direct elliptic solver, known as Stabilized Error Vector Propagator (SEVP).

Recently, Hatanaka and Kawahara [12] have investigated the flow behavior to find a critical value of Richardson number, when the flow changes from a periodic to a twin vortex pattern for a Reynolds number of 100. In an earlier study, vortex shedding behind a circular cylinder has been numerically simulated by a velocity correction method by Patnaik et al. [13] without considering the influence of buoyancy. Gowda et al. [14] have used the same algorithm for simulating the fluid flow and heat transfer past a tube bundle, by exploiting the symmetry in the flow domain. In both these earlier studies, the time discretization is performed by Eulers forward differencing procedure, which is only first-order accurate. The scheme employed in the present study has a second-order temporal accuracy. However, despite all these studies, it is not clearly known, if the phenomenon of vortex shedding could be triggered at low Reynolds numbers (for Reynolds numbers less than 40), where there are only twin vortices in the wake. To explore this objective, numerical investigations are carried out at these low Reynolds numbers to simulate the flow past a heated/cooled cylinder under the influence of buoyancy. Numerical flow visuals are drawn in the form of streaklines and streamlines to study the detailed near wake patterns. Lift and drag forces are computed from the velocity and pressure distributions. The relevant design parameters of interest related to heat transfer coefficients are also obtained.

2. Governing equations and boundary conditions

The governing equations are, the time dependent Navier–Stokes, continuity and energy equations, applicable for two-dimensions. The flow is assumed to be Boussinesq approximated, laminar and incompressible. The non-dimensional form of these equations are given by,

$$\frac{\partial u}{\partial x}+\frac{\partial v}{\partial y}=0 \tag{1}$$

$$\frac{\partial u}{\partial t}+u\frac{\partial u}{\partial x}+v\frac{\partial u}{\partial y}=-\frac{\partial p}{\partial x}+\frac{1}{Re}\nabla^2 u+Ri\,\theta \tag{2}$$

$$\frac{\partial v}{\partial t}+u\frac{\partial v}{\partial x}+v\frac{\partial v}{\partial y}=-\frac{\partial p}{\partial y}+\frac{1}{Re}\nabla^2 v \tag{3}$$

$$\frac{\partial \theta}{\partial t}+u\frac{\partial \theta}{\partial x}+v\frac{\partial \theta}{\partial y}=\frac{1}{Re\cdot Pr}\nabla^2\theta \tag{4}$$

The flow domain of interest with boundary conditions is depicted in Fig. 1. Here, the in-flow boundary is specified with a freestream velocity. The top and bottom boundaries are located at a transversal distance of ten times the cylinder diameter, where freestream velocity ($u=1.0$ and $v=0.0$) is imposed. The out-flow boundary is located such that, it does not influence the vortices formed in the near wake of the cylinder. This is naturally incorporated and arises in the context of finite element method, as applied to Navier–Stokes equations. The out-flow boundary condition is of the form,

$$-p+\frac{1}{Re}\left(\frac{\partial u}{\partial x}\right)=0.0;\quad \frac{1}{Re}\left(\frac{\partial v}{\partial x}\right)=0.0;$$

$$\frac{1}{Re\cdot Pr}\left(\frac{\partial \theta}{\partial x}\right)=0.0$$

Thus, a homogeneous Neumann boundary condition is naturally incorporated with a traction free exit. Further, it should be mentioned that the above equation is implemented in a weak fashion rather than in a pointwise manner. No-slip ($u=v=0.0$) is satisfied on the cylinder surface. The non-dimensional temperature of the in-flow (θ_∞) is imposed as 0.0 and that of the cylinder surface (θ_c) as 1.0. However, for the sake of clarity and simplicity in computations, heating or cooling of the cylinder surface is taken care of by expressing it by the directional influence of the buoyant forces. The Richardson number ($Ri=Gr/Re^2$) is taken as positive, when the cylinder is heated; and as negative, when it is cooled.

The algorithm employed in the present study is a modified velocity correction method of Ren and Utnes [15], which is essentially an extension of the popular projection scheme of Chorin [16]. In this scheme, the time integration is based on a R–K mid-point procedure, which is second-order accurate. Finite element spatial discretization is performed by the Galerkin

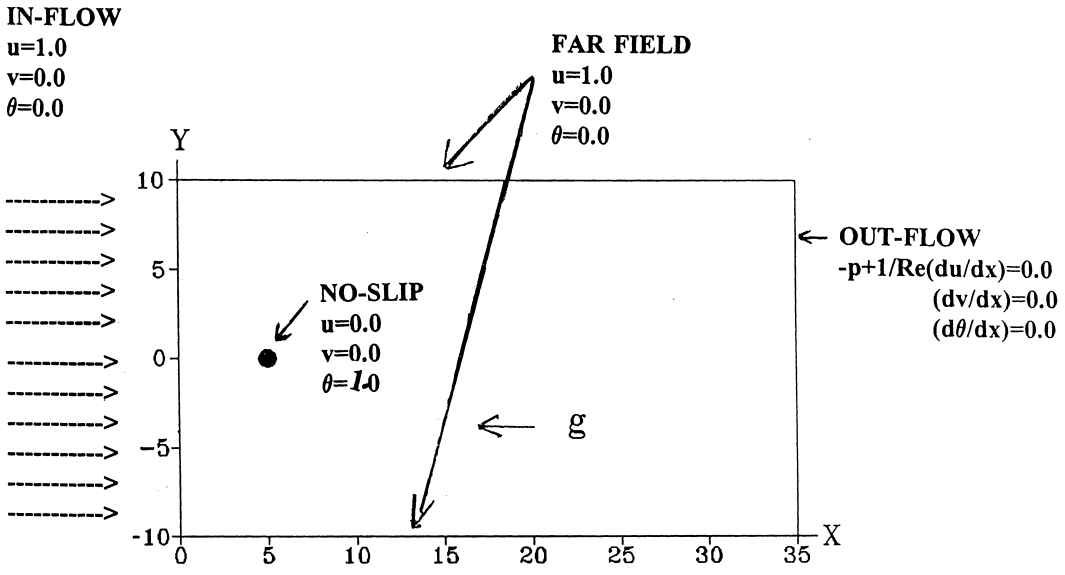

Fig. 1. Flow domain with boundary conditions.

weighted residual formulation with linear triangular elements. The following five steps are repeated within each iteration.

(1) Calculation of R–K coefficients (K_1, K_2) in order to obtain an intermediate velocity field ($\tilde{u}$), by omitting the pressure and force terms.

$$K_1 = \Delta t\left(\frac{1}{Re}\nabla^2 u^n - (u^n\nabla)u^n\right) \tag{5}$$

$$u_k = ((u^n) + K_1) \tag{6}$$

$$K_2 = \Delta t\left(\frac{1}{Re}\nabla^2 u_k - (u_k\nabla)u_k\right) \tag{7}$$

(2) Calculation of the intermediate velocity field.

$$\tilde{u} = (u^n) + \frac{(K_1 + K_2)}{2} \tag{8}$$

(3) Solving for pressure from the Poisson equation.

$$\nabla^2 P^n = \frac{1}{\Delta t}(\nabla\cdot\tilde{u}) \tag{9}$$

(4) Correction to the intermediate velocity field.

$$u^{n+1} = \tilde{u} - \Delta t(\nabla P^n - A) \tag{10}$$

where $\mathbf{u} = (u, v)$, $A = \langle Ri\ \theta, 0\rangle$.

(5) Obtaining the temperature field.

$$\theta^{n+1} = \Delta t\left(\frac{1}{Re\cdot Pr}\nabla^2\theta^n - (u^n\nabla)\theta^n\right) \tag{11}$$

The finite element spatial discretization is performed by the Galerkin weighted residual formulation, where the shape function itself is the weighing function. Linear triangular elements are used to represent U, V, P and θ, which are approximated as

$$U = N_iU_i + N_jU_j + N_kU_k$$

$$V = N_iV_i + N_jV_j + N_kV_k$$

$$P = N_iP_i + N_jP_j + N_kP_k$$

$$\theta = N_i\theta_i + N_j\theta_j + N_k\theta_k \tag{12}$$

Details of the formulation are as in Fletcher [17] and the shape functions defined for the triangular elements are as in Segarlind [18] and is elaborated in Patnaik [19]. After obtaining the velocity field, the stream function Eq. (13) is solved with appropriate boundary conditions to obtain the values of ψ for the entire fluid flow domain. The distribution of ψ is used in obtaining the streamline patterns.

$$\frac{\partial^2\psi}{\partial x^2} + \frac{\partial^2\psi}{\partial y^2} = -\left[\frac{\partial v}{\partial x} - \frac{\partial u}{\partial y}\right] \tag{13}$$

3. Results and discussion

The parameters chosen for the present investigation of simulating the wake behind a heated/cooled circular cylinder are as follows. A Richardson number

($Ri = Gr/Re^2$) variation of -1.0 to $+1.0$ is chosen for the analysis. For a Reynolds number of 40, it limits the Grashof number range from -1600 to $+1600$. This range is chosen such that, the limit imposed by the Boussinesq approximation is satisfied and the product of 'β' and 'ΔT' does not exceed 0.1. A Prandtl number of 0.71 is chosen, which renders an equivalent Peclet number ($Pe = Re \cdot Pr$) of 28.4 for $Re = 40$. A heated cylinder refers to buoyancy aiding the flow, while a cooled cylinder indicates that, it is opposing the flow. $Ri = 0.0$, refers to a pure forced convection situation in the absence of buoyancy.

The discretization process involves a certain amount of error which can be systematically reduced, at least in principle, by a series of grid refinements. The following three meshes have been chosen for the grid sensitivity analysis so as to check for the self consistency of the present study.

(A) 1464 nodes; 2872 elements
(B) 2124 nodes; 4298 elements
(C) 2568 nodes; 5476 elements.

By conducting grid dependence studies, it was observed that, the computational results have shown a maximum difference of about 6% between 'A' and 'B' type grids, while less than 2%, between 'B' and 'C' type, with respect to the average values of Nusselt and Strouhal numbers. Hence, mesh 'B' is found to be adequate for the present simulation and hence, is standardized for further analysis.

3.1. Fluid flow aspects

Fig. 2, shows the time averaged mean center line velocities along the axis of the cylinder in the wake region. This region is marked by a zone of reverse flow very near to the cylinder surface, which can be seen in the form of negative velocity values. The experimental observations of Griffin and Votaw [20] and Chilukuri [21] are also presented for the purpose of comparison. The present results compare well with the experimental investigations, particularly in the middle wake region.

3.1.1. Streamlines and streaklines

Streamlines indicate the flow pattern at a given instant of time. The influence of buoyancy on the fluid flow in the wake region is shown by plotting the instantaneous streamlines (Fig. 3), for $Ri = -1.0$, -0.25, 0.0, $+0.25$ and $+1.0$. Here, the angle of separation (ϕ_{sep}) measured from the forward stagnation point is lowest for $Ri = -1.0$, as the direction of flow and buoyancy oppose each other. The sinuous motion can be seen in the wake region, for $Ri = -0.25$ and -1.0. However, only two Föppl vortices are seen for $Ri = 0.0$ (pure forced convection case). Further, both the vortices vanish when the flow and buoyancy are in the same direction ($Ri = +1.0$). However, the capability of the streamlines to project the spatio-temporal history of the wake is limited. Hence, a particle release technique (similar to dye release in the experiments) has been incorporated to study the patterns associated with the wake structures under the influence of buoyancy. In the near wake region of the cylinder, a number of locations are chosen and particles are released continuously with time and their current locations in the flow domain are updated with progress in time. A novel bookkeeping procedure is employed to reduce the 'search-time' in locating the updated positions of these particles. Interestingly, these particles imbibe the history and transport effects associated with vortex shedding and buoyancy.

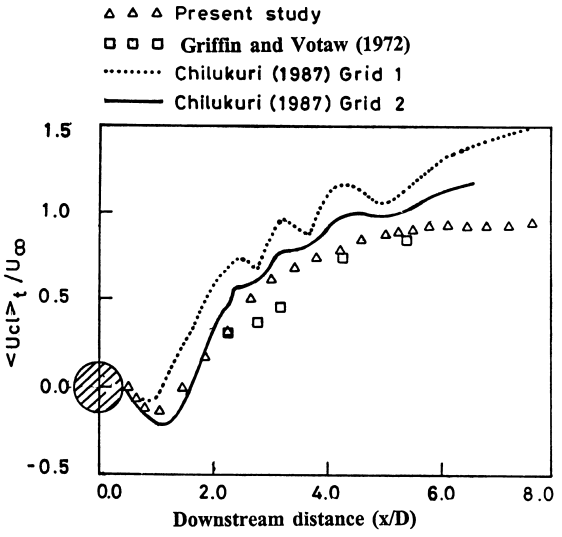

Fig. 2. Variation of time averaged mean centerline velocities.

The near wake patterns, thus obtained can be seen in Fig. 4. As can be observed, the twin vortex pattern of an unheated cylinder for $Re = 40$, is severely altered by the buoyant force. Vortex shedding is triggered by the opposing buoyancy, for a Richardson number range of -1.0 to -0.1. Also, the structure of the wake, size of its vortices and the time period associated with the vortex shedding process are dependent on the Richardson number. As can be observed, the transversal distance between the conglomerate vortex structures, for a cooled cylinder decreases from $Ri = -1.0$ to -0.1. The degeneration of the twin vortices into 'no-vortices' in the wake region is observed for buoyancy aided convection (Fig. 4(f) i.e. for $Ri = +1.0$). Thus, the influence of buoyancy is better revealed in these streakline plots.

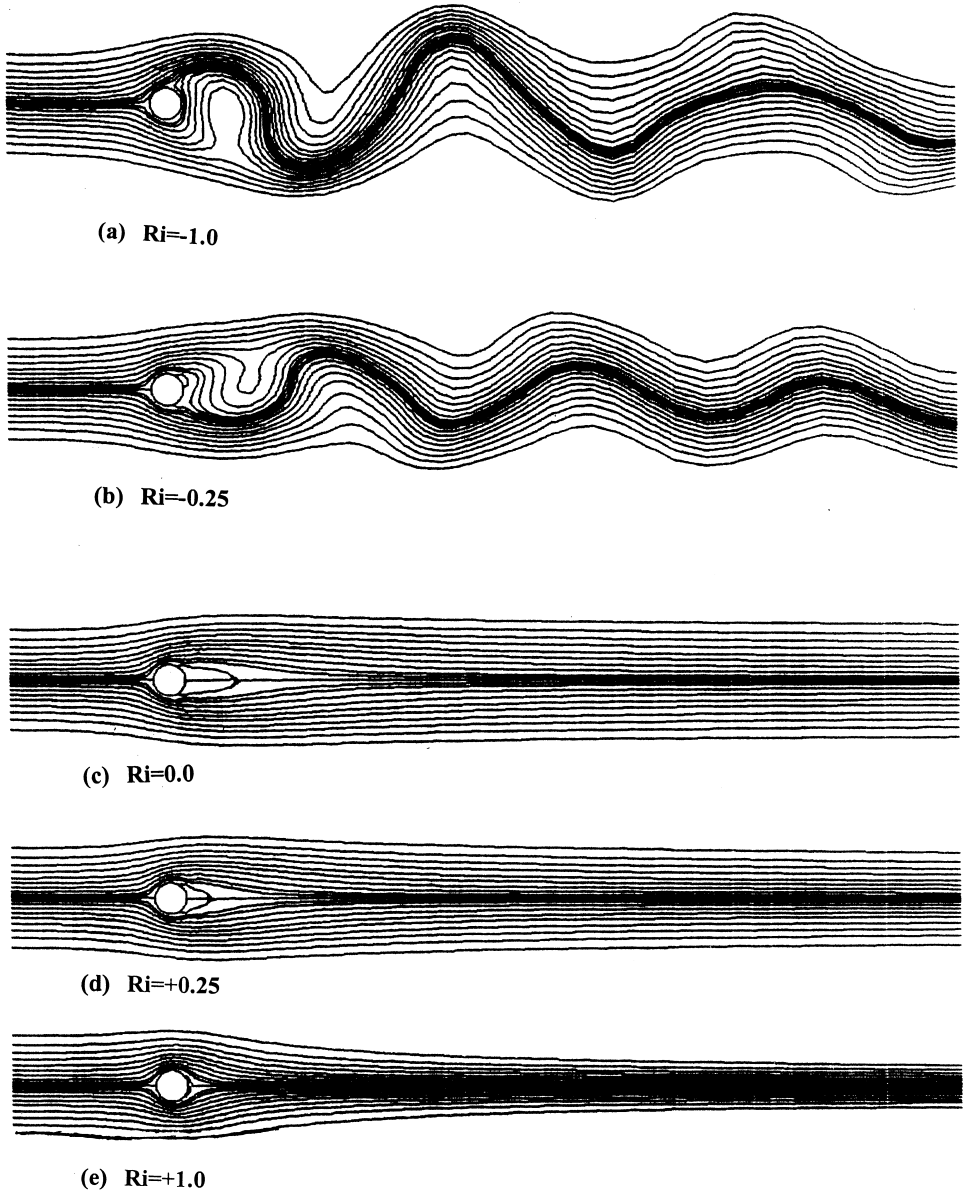

Fig. 3. Streamlines under the influence of buoyancy for $Re = 40$.

3.1.2. Lift and drag

The temporal lift and drag coefficient histories are determined from the velocity and pressure distribution in the flow domain. These are evaluated from the following relations:

$$C_l = -\int p \sin\theta \, d\theta + \frac{2}{Re}\int\left(\frac{\partial u}{\partial y} - \frac{\partial v}{\partial x}\right)\cos\theta \, d\theta$$

$$C_d = -\int p \cos\theta \, d\theta - \frac{2}{Re}\int\left(\frac{\partial u}{\partial y} - \frac{\partial v}{\partial x}\right)\sin\theta \, d\theta$$

The temporal variations in lift and drag coefficients can be seen in Fig. 5 for different Richardson number values for a fixed Reynolds number of 40. Drag coefficient is averaged over a number of vortex shedding cycles to obtain, $\overline{C_d}$, while, root mean square values are obtained from the lift coefficient histories. The values of average drag coefficient ($\overline{C_d}$) against the Reynolds number for $Ri = 0.0$ is shown in Fig. 6. It shows a good correspondence with the available experimental and numerical investigations.

In the Richardson number range of -1.0 to $+1.0$

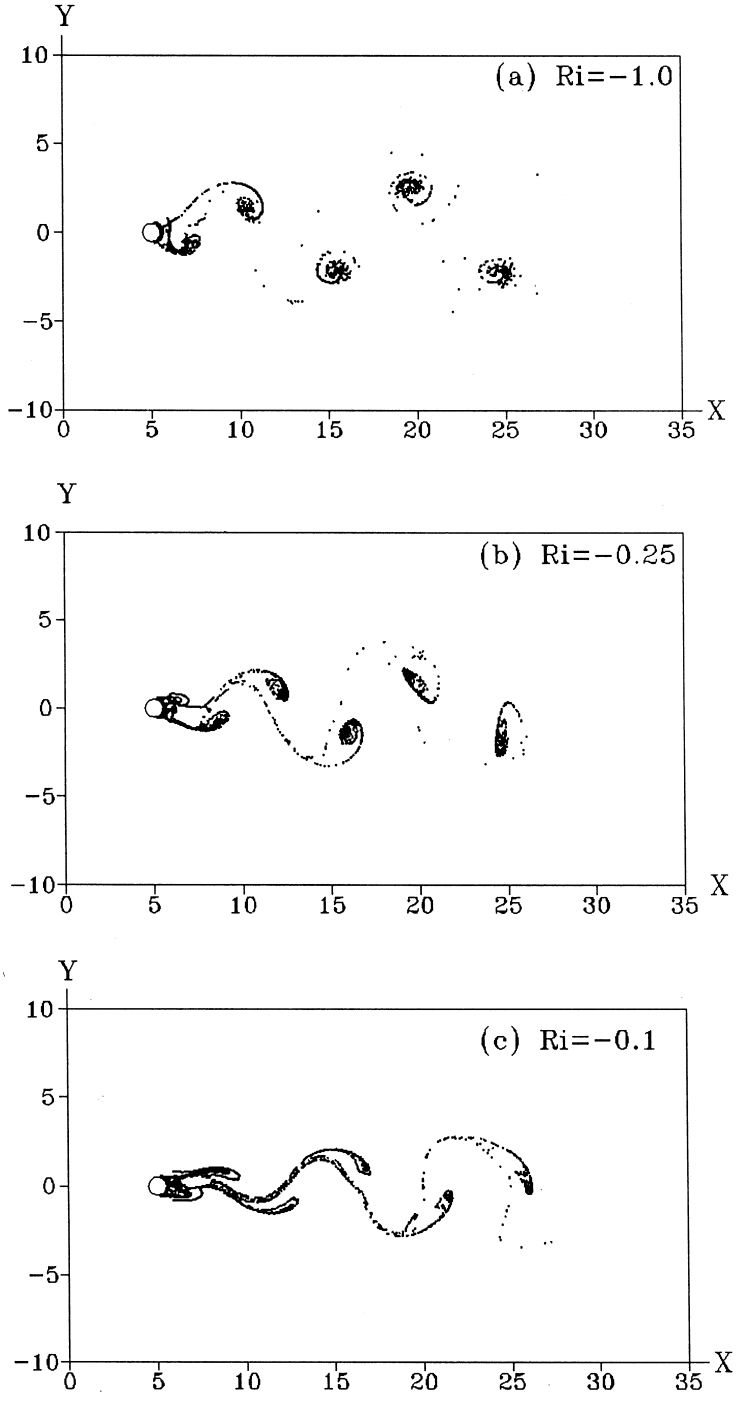

Fig. 4. Wake structure under the influence of buoyancy for $Re = 40$.

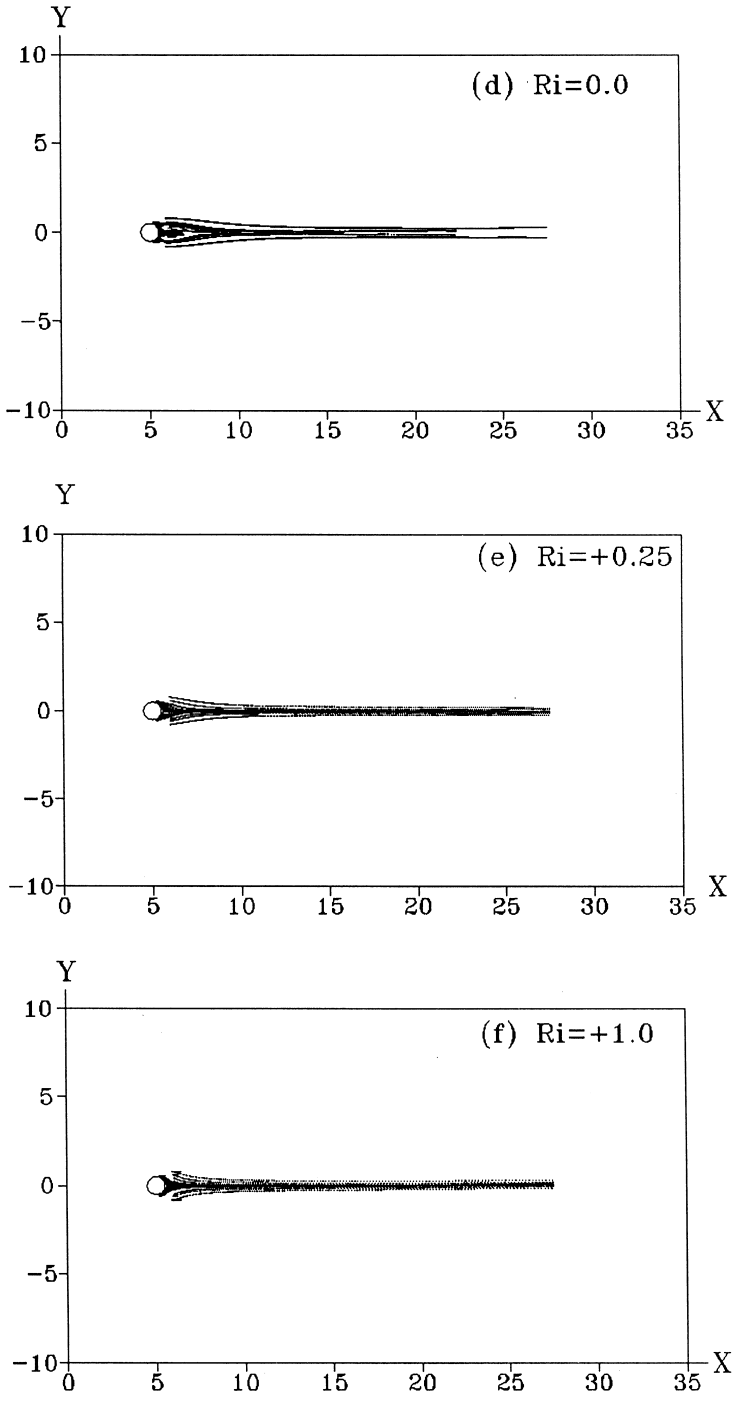

Fig. 4 (*continued*)

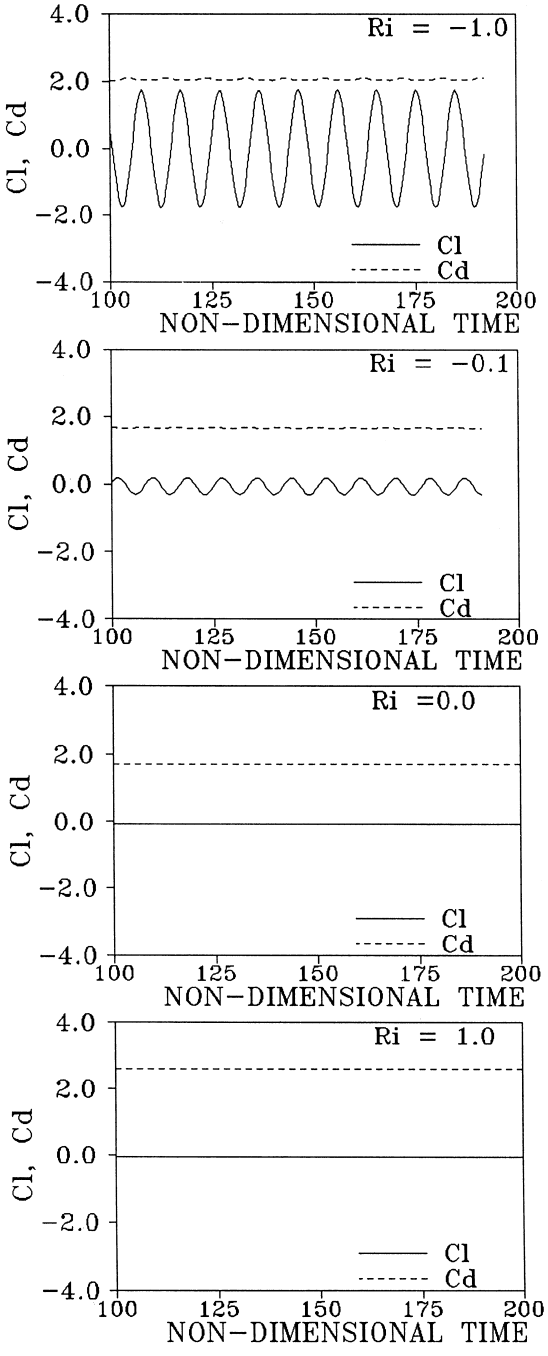

Fig. 5. Temporal variation of lift and drag coefficients for $Re = 40$.

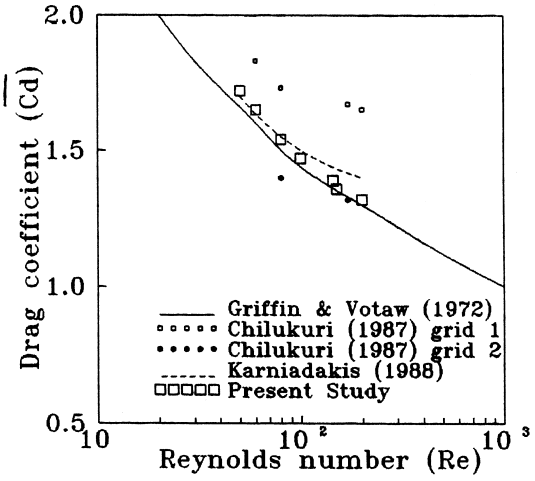

Fig. 6. Comparison of average drag coefficient over a range of Reynolds numbers.

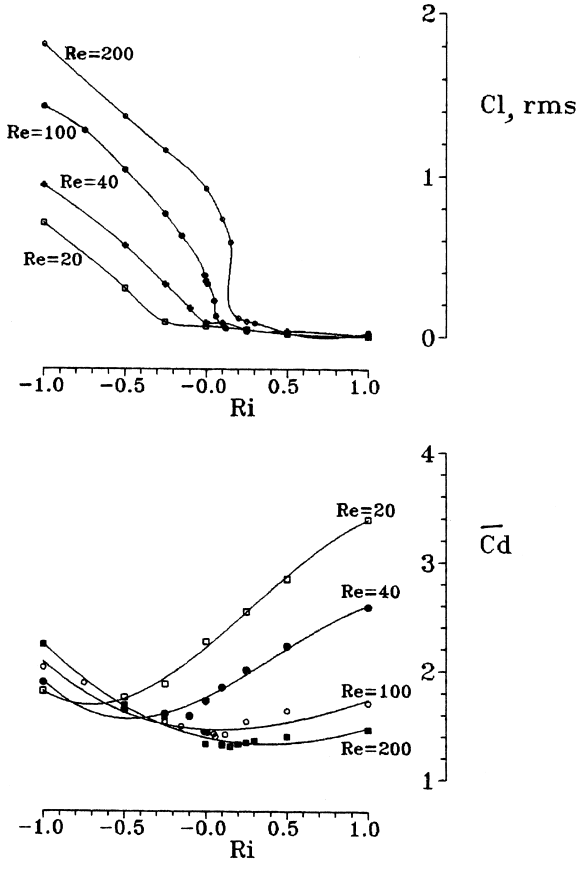

Fig. 7. Variation of RMS lift and average drag coefficients.

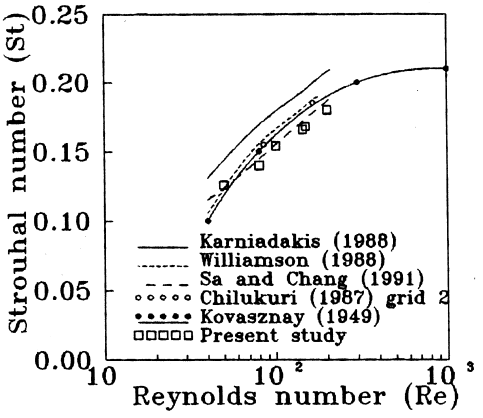

Fig. 8. Comparison of Strouhal number against Reynolds number.

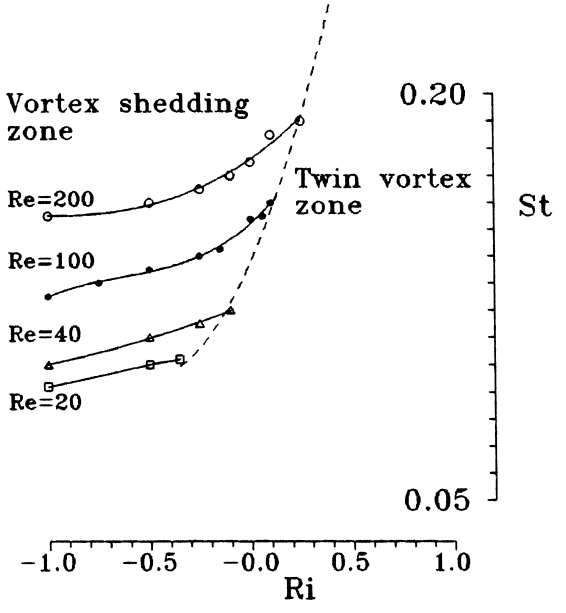

Fig. 9. Strouhal number variation with Richardson number.

the variation of $\overline{C_d}$ and $C_{1,rms}$ values are plotted in Fig. 7. As can be observed, the average drag coefficient for $Re=20$ and 40 increases with an increase in Ri, while it decreases for $Re=100$ and 200. This interesting anomaly may be explained from the wake patterns that result due to the influence of buoyancy. For $Re=20$–40, there are twin vortices in the wake region, under pure forced convection (i.e. $Ri=0.0$). When the Richardson number variation is from 0.0 to +1.0 (buoyancy aiding the flow), the separation points move towards the aft. It is known that the total drag comprises of drag due to skin friction and pressure drop. For these two low Reynolds numbers ($Re=20$ and 40), contribution due to skin friction increases substantially with an increase in Ri, while that due to pressure drop, decreases marginally. Interestingly, the sum of these two components, which comprises the total drag increases. On the contrary, for $Re=100$ and 200, an eddy roll-up process exists in the wake of the circular cylinder, even when there is no influence due to buoyancy ($Ri=0.0$). The point of separation moves towards the upstream for a cooled cylinder ($-1.0 < Ri < 0.0$), while it moves towards the downstream for a heated body ($0.0 < Ri < +1.0$). This flow separation results in a wider wake for the cooled cylinder and a narrower wake for the heated one. Consequently, the drag coefficient is higher, when the cylinder is cooled, than when it is heated, which is due to a higher contribution from the form drag.

The influence of buoyancy contributes to the undulations in the wake of a circular cylinder, influencing the wake patterns. This is indirectly depicted in the $C_{1,rms}$ plot (Fig. 7). For $Re=100$ and 200, there is a sharp drop (around $Ri=+0.12$) in $C_{1,rms}$ values due to the degeneration of the Kàrmàn vortex street into twin vortices. The lift force is also induced for $Re=20$ and 40, when buoyant force and the flow direction oppose each other. Further, the curves are flat indicating that, only a negligible amount of lift force is induced.

3.1.3. Vortex shedding frequency

The Strouhal number (St) is a measure of the oscillating fluid flow phenomenon in the wake region, and is connected to the fluid flow parameters by the following relation

$$St = \frac{f_{vs}{}^{*} D}{U_\infty}$$

where f_{vs} is the vortex shedding frequency, D, is the diameter of the cylinder, and U_∞, is the freestream velocity. When U_∞, and D are non-dimensionalized as unity, St is equivalent to f_{vs}. Thus, the Strouhal number is obtained as the inverse of the time period of vortex shedding (T_{ps}). In the present study, Strouhal numbers are deduced both from the signal traces of the monitored velocity fluctuations and also from the temporal lift force coefficients. Strouhal numbers obtained from the present analysis is compared with some of the existing experimental and numerical investigations and can be seen in Fig. 8 for $Ri=0.0$. A good comparison can be noticed with Refs. [22–25]. When the cylinder is cooled below the ambient temperature ($-1.0 < Ri < 0.0$), the strength of the shear layer increases and the eddy roll-up process is more activated as the velocity in the wake region is reduced by the buoyancy opposed convection of the cold air. Hence, flow separation takes place much earlier than usual, resulting in a higher wake width. On the con-

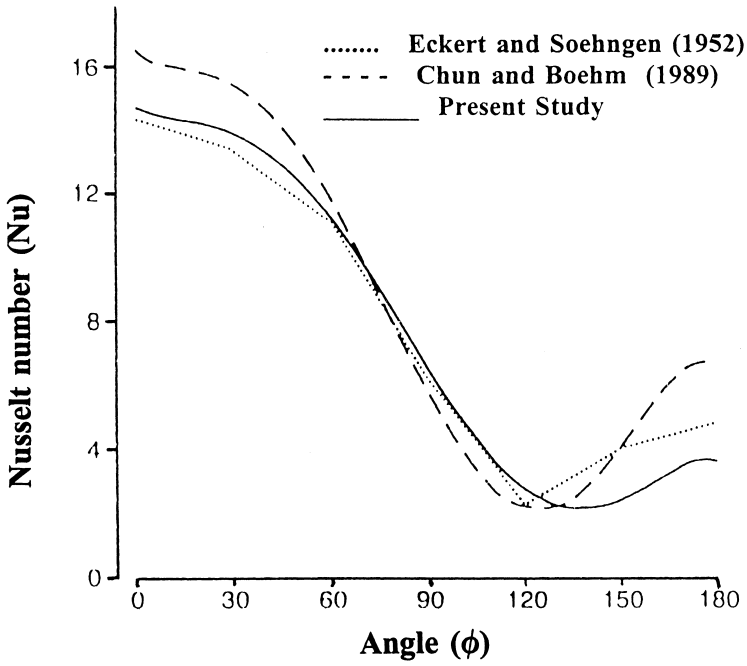

Fig. 10. Comparison of local Nusselt number for $Re = 200$.

trary, heating ($0.0 < Ri < +1.0$) increases the velocity in the wake region and causes the shear layer to be weakened. This is due to the fact that, the entrainment of the ambient fluid into the wake cavity is less easy, and results in a faster vortex shedding. Further, it can be observed in Fig. 9, that the frequency of vortex shedding is a function of both Reynolds and Richardson numbers. While heating accelerates the boundary layer formed on the cylinder surface and hastens the vortex shedding process, cooling impedes the rate of eddy roll-up. Increase in the values of Strouhal numbers can be noticed with Richardson numbers. However, beyond a certain range of Richardson numbers, only the presence of twin vortices are seen instead of a vortex street. This process has been experimentally observed by Noto and Matsumoto [10] and they called it the 'breakdown of the Kàmàn vortex street'. The two zones viz vortex shedding zone and the twin vortex zone are clearly demarcated in Fig. 9. While a steady state solution exists towards the right of the curve (twin vortex zone), it is marked by a periodic phenomena on the left (vortex shedding zone). Interestingly, for a certain Richardson number range, even the twin vortex pattern eventually vanishes. The numerical flow visuals of Hatanaka and Kawahara [12], have established that for a Reynolds number of 100, at $Ri = +0.125$ the vortex shedding process ceases. The corresponding value obtained from the present study is $Ri = +0.12$, which is in good conformity with this earlier investigation.

3.2. Heat transfer aspects

3.2.1. Nusselt number and temperature distribution

A knowledge of the heat transfer coefficients at low Reynolds numbers is invaluable to designers, mainly due to the use of hot wires or films in velocity measurement. As the diameter of these elements correspond to small Reynolds numbers, the influence of buoyancy cannot be neglected. Here, the Nusselt number is the design parameter of interest. The local Nusselt number distribution is obtained by calculating the temperature gradient on the circular cylinder from the following relation

$$Nu_{\text{local}} = \left.\frac{\partial \theta}{\partial y}\right|_{\text{wall}}$$

Fig. 10 depicts the local Nusselt number variation for flow past an isothermal circular cylinder in an infinite medium for $Re = 200$. It is compared with the experimental results of Eckert and Soehngen [2] and finite difference results of Chun and Boehm [26]. Due to smaller thermal resistance, the local Nu at the forward stagnation point is highest and decreases up to the point of separation. In the wake region, where the vortices are formed and shed, a further increase in the Nusselt number can be seen because of good mixing. Due to the influence of vortex shedding, the local Nusselt number distribution in the wake region varies temporally in the downstream region. However, these

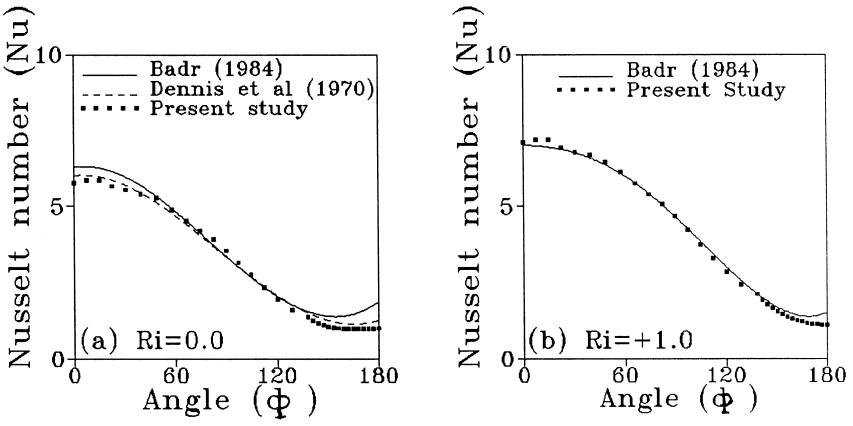

Fig. 11. Comparison of local Nusselt number for $Re=40$.

variations are averaged out for the purpose of comparison. The present finite element predictions compare well with the experimental values up to the point of separation. Even beyond the point of separation, the present results are closer to the experimental values than the finite difference predictions of Chun and Boehm [26].

Under the influence of gravity, the induced buoyant forces have a substantial influence at low Reynolds numbers. Hence, in the present study, the influence of buoyancy is studied by varying the Richardson number. A comparison of local Nu distribution for $Re=40$, is shown in Fig. 11. The Nusselt number decreases from a maximum at the upstream stagnation point to a minimum towards the downstream, as a continuously drooping curve. Further, Fig. 11, also shows a higher heat transfer for $Ri=+1.0$ (Fig. 11(a)), in comparison with its corresponding value for $Ri=0.0$ (Fig. 11(b)). Here, the angle (ϕ) varies between 0 and 180° on the abscissa against the Nusselt number on the ordinate. A comparison with the available analytical studies of Dennis and Chang [27] and Badr [28] shows a good prediction. For different Richardson numbers (both positive and negative) local Nusselt number values are plotted. This variation under the influence of buoyancy can be seen in Fig. 12. Here, it should be mentioned that, $Ri=+0.25$ and $+1.0$ correspond to the cases of flow aiding buoyancy, while $Ri=-0.25$ and $Ri=-1.0$ refer to the cases of flow opposing buoyancy. When the flow and the force of buoyancy are in the same direction, the thermal boundary layer is thinner and hence, there is a higher heat transfer coefficient. However, it becomes thicker when they oppose each other. Due to the influence of natural convection over the forced flow, more intense fluid dynamical activity in the downstream region causes vortex shedding behind the circular cylinder. As the vortices are formed and shed, a better mixing is possible in the separated flow region, which in turn allows a marginal increase in the local values of the Nusselt number for $Ri=-1.0$ and -0.25.

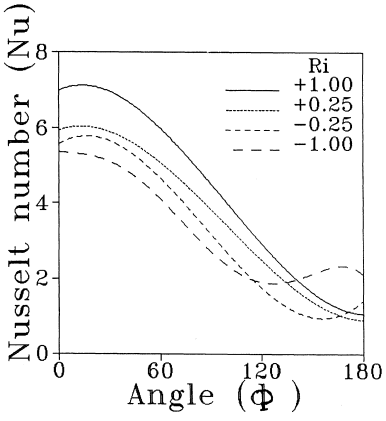

Fig. 12. Influence of Richardson number on the local Nu for $Re=40$.

Isotherms for different Richardson numbers corresponding to a fixed Reynolds number of 40 are presented in Fig. 13. These isotherms, which represent the movement of heat flow at a particular instant of time, depict a periodic behavior for $Ri=-1.0$ and -0.25, while remain steady for $Ri=0.0$, $+0.25$ and $+1.0$. Thermal boundary layer growth symmetrically starts at the forward stagnation point and becomes thicker towards the aft. On the upstream side, the distribution is regular and packed, while in the downstream, the influence of vortex shedding on the flow patterns is clearly depicted in the migration of these isotherms as in Fig. 13(a) and (b). Here, isotherms show a periodic movement due to the oscillatory nature of the wake region. Primarily, the value of the Richardson number governs the behavior of the isothermal pattern beyond the point of boundary layer separation.

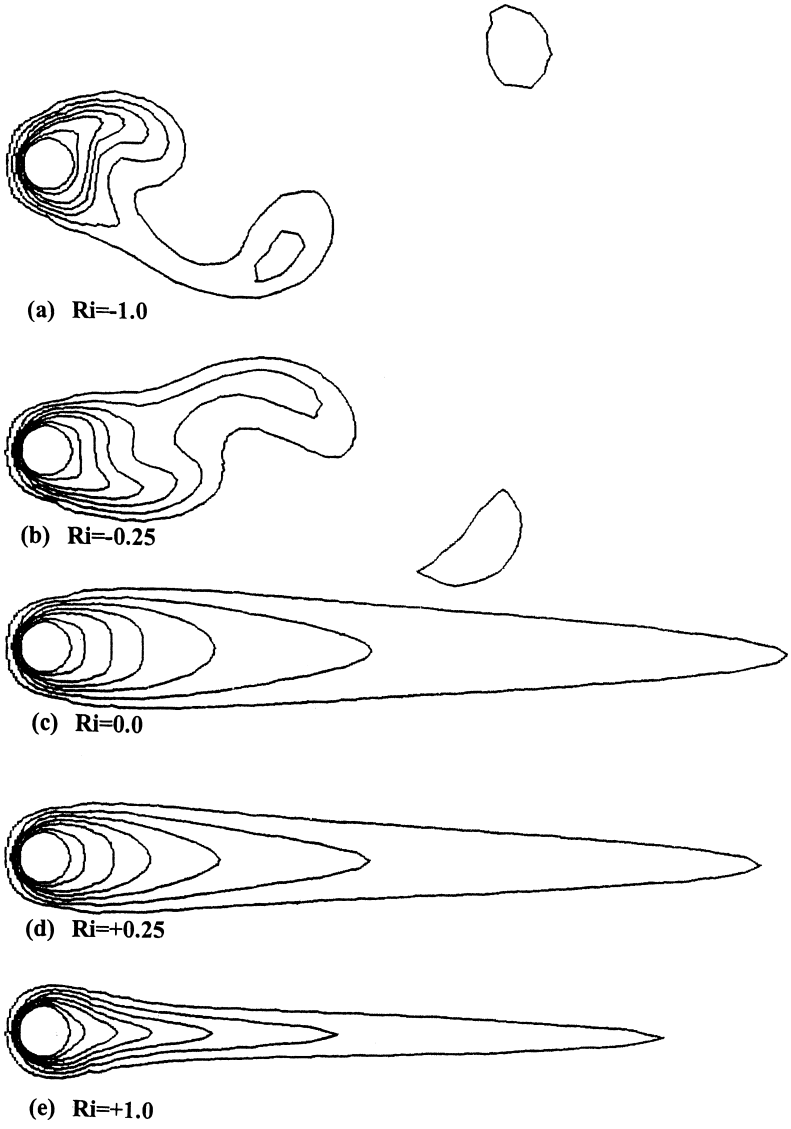

Fig. 13. Isotherms for $Re = 40$ (values: 1.0, 0.9, 0.8, 0.7, 0.5, 0.4 and 0.3 over the cylinder surface to the outermost contour).

4. Summary and conclusions

The influence of buoyancy aiding or opposing the flow direction is numerically simulated for flow past a circular cylinder. A modified velocity correction procedure with R–K time integration, and a finite element based Galerkin weighted residual formulation are incorporated. The influence of buoyancy on the Nusselt number, Strouhal number, structure of the wake, lift and drag forces, etc. has been investigated. A numerical way of releasing the particles is implemented to visualize the fluid flow structure of the wake region. Some of the broad conclusions can be outlined as follows:

- Under the influence of buoyancy opposed convection, vortex shedding could be triggered at low Reynolds numbers of $Re = 20$–40, where there are only twin vortices in a natural way. Even the twin vortices formed in the wake have totally vanished for certain cases of buoyancy aided convection.
- In the Reynolds number range of 100–200, the eddy roll-up process is weakened due to heating, until the dynamic vortices finally degenerate into Föppl vortices.
- Flow past a cooled circular cylinder results in a wide wake due to greater entrainment from the ambient fluid, while heating narrows the same due to delayed separation.

- The zones for vortex shedding and twin vortices are clearly demarcated in the plot of Reynolds number against Strouhal number.

Acknowledgements

The authors thank the referees for their invaluable suggestions.

References

[1] E. Berger, R. Wille, Periodic flow phenomena, Annual Reviews of Fluid Mechanics 4 (1972) 313–340.
[2] E.R.G. Eckert, E. Soehngen, Distribution of heat transfer coefficient around circular cylinders in cross flow at Reynolds numbers from 20 to 500, Transactions of ASME Journal of Heat Transfer 101 (1952) 343–347.
[3] B.E. Eaton, Analysis of laminar vortex shedding behind a circular cylinder by computer-aided flow visualization, Journal of Fluid Mechanics 180 (1987) 117–145.
[4] G.K. Sharma, S.P. Sukhatme, Combined free and forced convection heat transfer from a heated tube to a transverse air stream, Transactions of ASME Journal of Heat Transfer 91 (1969) 457–459.
[5] P.H. Oösthuizen, S. Madan, Combined convective heat transfer from horizontal circular cylinders in air, Transactions of ASME Journal of Heat Transfer 92 (1970) 194–196.
[6] N.D. Joshi, S.P. Sukhatme, An analysis of combined free and forced convection heat transfer from a horizontal circular cylinder to a transverse flow, Transactions of ASME Journal of Heat Transfer 93 (1971) 441–448.
[7] E.M. Sparrow, L. Lee, Analysis of a mixed convection about a horizontal cylinder, International Journal of Heat and Mass Transfer 19 (1976) 229–231.
[8] J.H. Merkin, Mixed convection from a horizontal circular cylinder, International Journal of Heat and Mass Transfer 18 (1977) 73–77.
[9] P.C. Jain, B.L. Lohar, Unsteady mixed convection heat transfer from a horizontal circular cylinder, Transactions of ASME Journal of Heat Transfer 101 (1979) 126–131.
[10] K. Noto, M. Matsumoto, Generation and suppression of the Kàrmàn vortex street upon controlling surface temperature of a cylinder, Proceedings of Numerical Methods Laminar and Turbulent Flows 7 (1991) 671–678.
[11] K.S. Chang, J.Y. Sa, The effect of buoyancy on vortex shedding in the near wake of a circular cylinder, Journal of Fluid Mechanics 220 (1990) 253–260.
[12] K. Hatanaka, M. Kawahara, Numerical study of vortex shedding around a heated/cooled circular cylinder by the three step Taylor–Galerkin method, International Journal for Numerical Methods in Fluids 21 (1995) 857–867.
[13] B.S.V.P. Patnaik, K.N. Seetharamu, P.A. Aswatha Narayana, Simulation of laminar confined flow past a circular cylinder with integral wake splitters involving heat transfer, International Journal of Numerical Methods for Heat and Fluid Flow 6 (4) (1996) 65–81.
[14] Y.T.K. Gowda, B.S.V.P. Patnaik, P.A. Aswatha Narayana, K.N. Seetharamu, Finite element simulation of transient laminar flow and heat transfer past an in-line tube bank, Journal of Heat and Fluid Flow 19 (1) (1998) 49–55.
[15] G. Ren, T. Utnes, A finite element solution of time-dependent incompressible Navier–Stokes equations using a modified velocity correction method, International Journal for Numerical Methods in Fluids 17 (1993) 349–364.
[16] A.J. Chorin, Numerical simulations of Navier–Stokes equations, Mathematical Computations 22 (1968) 745–762.
[17] C.A.J. Fletcher, Computational Galerkin Methods, Springer-Verlag, New York, 1984.
[18] L.J. Segarlind, Applied Finite Element Analysis, Wiley, New York, 1984.
[19] B.S.V. Patnaik, Finite element analysis of flow past a circular cylinder and two cylinders in tandem: influence of vibration, buoyancy, Ph.D. thesis, IIT, Madras, India, 1998.
[20] O.M. Griffin, C.W. Votaw, The vortex street in the wake of a vibrating cylinder, Journal of Fluid Mechanics 51 (1) (1972) 31–48.
[21] R. Chilukuri, Incompressible laminar flow past a transversely vibrating cylinder, Transactions of ASME Journal of Fluids Engineering 109 (1987) 166–171.
[22] G.M. Karniadakis, Numerical simulation of forced convection heat transfer from a cylinder in cross flow, International Journal of Heat and Mass Transfer 31 (1) (1988) 107–118.
[23] C.H.K. Williamson, Defining a universal and continuous Strouhal relationship for the laminar vortex shedding of a circular cylinder, Physics of Fluids 31 (10) (1988) 2742–2744.
[24] J.Y. Sa, K.S. Chang, Shedding patterns of near wake vortices behind a circular cylinder, International Journal for Numerical Methods in Fluids 12 (1991) 463–474.
[25] L.S.G. Kovasznay, Hot wire investigation of the wake behind cylinders at low Reynolds numbers, Proceedings of the Royal Society Series A 198 (1949) 174–190.
[26] W. Chun, R.F. Boehm, Calculation of forced flow and heat transfer around a circular cylinder, Numerical Heat Transfer 15 (1989) 101–122.
[27] S.C.R. Dennis, G.Z. Chang, Numerical solution of steady flow past a circular cylinder at Reynolds numbers up to 100, Journal of Fluid Mechanics 42 (1970) 471–489.
[28] H.M. Badr, Laminar combined convection from a horizontal cylinder—parallel and contra flow regimes, International Journal of Heat and Mass Transfer 27 (1) (1984) 15–27.